Research Article

Combined droop nose and trailing-edges morphing effects on airfoils aerodynamics

M. A. Aziz[1] · M. Mansour[2] · D. Iskander[2] · A. Hany[3]

Abstract

Airfoils' morphing offers benefits to traditional aerodynamics characteristics flight such drag saving and better maneuver skills for aircrafts by different means. The current study introduces a parametric optimization for the effect of droop nose and trailing-edges morphing on airfoils aerodynamics characteristics. The study has conducted using the X-FOIL imported in MATLAB program and ANSYS Fluent software. The first used as a prelude parametric study for the numerical simulations. The morphed airfoil configuration parameterized with four variables: leading and trailing edges deflections, δ_1, δ_2 and the morphing lengths E_1, E_2. The results from X-FOIL showed increase in stall angle up to 26° and lift to drag ratio up to 120. The more accurate simulation results showed increase of stall angle up to 20° and lift to drag ratio increased up to 6.22% compared to basic airfoil at separate morphed shapes. The lift coefficient increased also up to 1.34. The study also introduces morphing control to insure maximum lift coefficient during the variety of operating angle of attack.

Keywords Morphing · Droop nose · Trailing-edges · Experimental measurement · Aerodynamic control

1 Introduction

The high-lifting devices in air craft such flaps, slats and ailerons represent overweight and extra complexity. This extra weight of the mechanism, complexity of the operating and control systems is a problem from the design and operation point of view. By itself, the overall system complexity and structure weight are considerably increased. Unlike conventional wing control surfaces, morphing leading-edge and trailing-edge usually use the conformal structural deformation achieved through bending and twisting of structures to adaptively change wing shape, leading to potentially systems and reduced weight. Also, morphing allows a smooth change for geometry surface to outfit a certain aero load which is desirable for noise reduction.

Recent studies focused in such helpful method to improve the aerodynamic performance of different applications such wind energy, aircraft parts and component and etc. Yue et al. [1] have worked on aircraft maneuvering enhancement using morphing wing by increasing the roll angular velocity. They have used the approximation of quasi steady aerodynamics. Kamliya et al. [2] have showed that morphing with higher camber flap increase the lift coefficient while a little decrease the lift to drag ratio is observed. Gamble et al. [3] have used morphing hinge at airfoil trailing edge which was capable of delay the inception of stall to higher angle of attack but with slight reduction in lift coefficient. Kimaru and Bouferrouk [4] have showed experimentally the wing with morphing camber which has a better aerodynamic performance for different angles of attack than traditional wings.

Aerodynamic performance enhancement and structural mass reduction have been introduced using morphing skill applied to airfoil camper Vale1 et al. [5]. Jodin et al. [6] have showed that vibrating the airfoil trailing edge with high frequency and little amplitude was capable of rising the lift and reducing the drag consequently. Vasista et al [7] have studied the wing tip droop-nose using morphing technique and explained experimentally the visions from tests and gave some recommendations also they were not envisioned to improve the wing aerodynamic loads coefficients. As they mentioned, their study has lacked of aerodynamic studies for the problem to determine the effect of droop-nose on the flying performance.

A saving in fuel consumption have been achieved using morphing wingtips and growth in yaw power using twisting morphing and bending morphing Afonso et al. [8]. Morphing wing applications have extended to growth the photo voltaic collected energy during small angle of sun rise by correcting dihedral angle of small wing part near tip with acceptable variant in aerodynamics loads Wu et al. [9]. Many studies have focused on nonlinearity of the morphing wings. Zhang et al. [10] have introduced dynamic analyses for deploying wings and aerodynamic improvement using the thin airfoil theory. Hu et al. [11] have presented some aero-elasticity features and responses of morphing wings.

The current study introduces the aerodynamic characteristics of morphing airfoil including droop nose and trailing edge morphing. The parametric optimization is performed first using X-FOIL-MATLAB followed by numerical simulation study with ANSYS Fluent software. The studies aims to improve aerodynamics characteristics flight such drag saving and peter maneuver skills for aircrafts by different means such delaying stall inception and enhance the aerodynamics coefficients compared to the original airfoil.

2 Parametric study for the variation

The predication for the aerodynamic characteristics are calculated using X-FOIL imported to MATLAB; the X-FOIL applies the vortex lattice method (VLM) in order to solve for the aerodynamic characteristics for a given airfoil. The VLM gives a good prediction for the aerodynamic performance and to indicate the trend of some variation on a certain airfoil. The reason to use the VLM is that the high computational cost of using the CFD, the prediction resulted from the VLM could narrow the working region in order decrease the number of runs to be done using the CFD. The accuracy X-FOIL in comparison with CFD and experimental measurements has presented by Günel et al. [12].

The study aims to improve important aerodynamic parameters such; $(C_L/C_D)_{MAX}$ and α_{STALL}. A parametric study is then conducted including sufficient number for different morphing geometries. A MATLAB script has been prepared to generate the morphed shape as function of four control parameters. The airfoil morphed profile is shaped using a deflection having a parabolic profile with three coefficients in which are calculated based on the E_1, E_2, δ_1 and, δ_2 values and the unmorphed profile of the airfoil. For the deflection which is denoted as δ for the leading edge:

$$\delta(x) = l_1 x^2 + l_2 x + l_3 \tag{1}$$

where l_1, l_2 and l_3 are constant to be determined by applying conditions at leading edge.

$$\frac{d\delta(x)}{dx} = 2l_1 x + l_2 \tag{2}$$

$$\delta(x) = \begin{cases} \delta_1 c, & x = 0 \\ 0, & x = E_1 c \end{cases} \tag{3}$$

where c is the airoil chord length

$$\frac{d\delta(E_1 c)}{dx} = \frac{dy_c(E_1 c)}{dx} \tag{4}$$

applying conditions,

$$l_3 = \delta_1 c \tag{5}$$

$$l_1 (E_1 c)^2 + l_2 (E_1 c) = -\delta_1 c \tag{6}$$

$$2l_1 (E_1 c) + l_2 = \frac{dy_c(E_1 c)}{dx} \tag{7}$$

$$\begin{bmatrix} l_1 \\ l_2 \end{bmatrix} = \begin{bmatrix} E_1^2 c^2 & E_1 c \\ 2E_1 c & 1 \end{bmatrix}^{-1} \begin{bmatrix} -\delta_1 c \\ \frac{dy_c(E_1 c)}{dx} \end{bmatrix} \tag{8}$$

Similarly for the trailing edge,

$$\begin{bmatrix} t_1 \\ t_2 \\ t_3 \end{bmatrix} = \begin{bmatrix} ((1-E_2)c)^2 & ((1-E_2)c) & 1 \\ c^2 & c & 1 \\ 2(1-E_2) & 1 & 0 \end{bmatrix}^{-1} \begin{bmatrix} 0 \\ \delta_2 c \\ \frac{dy_c((1-E_2)c)}{dx} \end{bmatrix} \tag{9}$$

where t_1, t_2 and t_3 are constant to be determined by applying conditions at trailing edge. Finally, considering the ranges discussed above the new profile becomes,

$$\begin{bmatrix} y_u \\ y_l \end{bmatrix}_{morphed} = \begin{bmatrix} y_u \\ y_l \end{bmatrix}_{clean} + \delta(x) \begin{bmatrix} 1 \\ 1 \end{bmatrix} \tag{10}$$

The current study intended on low speed aircraft up to 45 m/s flight speed and 1 km flight altitude where the

Reynolds number change did not exceed 5% for a unity chord length. For that the Reynolds number is considered constant during the different flight regimes. The study includes high lift generation flight regime during takeoff and maneuvering where the critical parameter is the stall angle of attack. Also, the cruise flight regime where the maximum lift coefficient and minimum drag coefficient are most preferred.

The morphed aerofoil nomenclature used in the analysis is presented in Fig. 1. Two sets of parameters have used during simulations, the first and second set of morphing parameters are presented in Table 1. The simulations have done at the following conditions: the Reynolds number $= 3 \times 10^6$, the density $\rho = 1.225$ kg/m^3, the inlet velocity $V = 43.822$ m/s.

Figures 2 and 3 summarize the results of the first and second set using contours for both stall angle of attack and the lift to drag ratio respectively. Each figure contains nine contours show the variation with the trailing edge deflections, δ_2 and the morphing length E_2, at a different leading edge deflection δ_1 and morphing length E_1. It is obvious that the trailing edge upward deflections mainly affects the stall angle of attack positively Fig. 2a, b, but as a cost for this, the $C_L/C_{D_{max}}$, decreases dramatically in which can be compensated using the downward leading edge deflection as shown in Fig. 3a, b.

The trailing edge deflection increased the stall angle of attack while it attenuated the $(C_L/C_D)_{MAX}$, the effect of E_2 is that the longer E_2 the lower stall angle of attack while it gives higher lift to drag ratio. This may be explained as the study combined effect of both δ_2 and E_2, at high angle of attack the separation appears near trailing edge. The deflected trailing edge works on better attachment for the flow at high angle of attack. The effect of a pure trailing edge deflection can be represented by the Table 2. The stall angle of attack didn't face any attenuation but
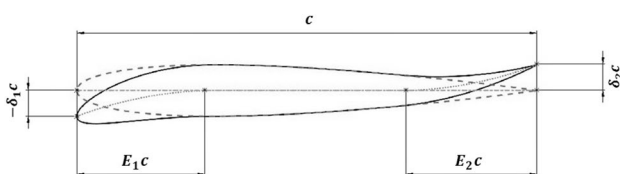
it increased. The remarkable point is that the $(C_L/C_D)_{MAX}$ has increased a lot more than that in case of a basic airfoil, the effect of increase of E_1 is that it mainly decreases the $(C_L/C_D)_{MAX}$, and has no remarkable effect on the stall angle of attack. The leading edge deflection effect can be shown by Table 3

It is concluded that the leading edge deflection compensated the attenuation in lift to drag ratio caused by the trailing edge deflection, and at a higher angle of attack, but the lift to drag still lower than the basic airfoil. The overall effect at the maximum leading and trailing edges deflections is represented by Table 4.

3 Numerical simulations

The numerical simulations have conducted using ANSYS Fluent for Newtonian flow. The software solves 2D Navier–Stokes equations, incompressible, steady-state fluid flow using finite volume technique. The simulations have performed using workstation with the following characteristics: Intel core i7, 5th generation, 3 GHz processor (cash 4 MB) and 16 GB RAM. The geometry has created by ANSYS design modeler and the mesh generation has conducted using ANSYS mesh modeler using unstructured mesh with some modifications around the airfoil to capture the boundary layer and flow separation.

4 Grid sensitivity and verification

The sensitivity analysis had conducted to increase the accuracy of the grid with the results (lift coefficient, Drag coefficient, Y+, etc.). The Y^+ is a good indication of grid quality. For low-Reynolds number turbulence models the Y+ value ≤ 1.0 Ariff et al. [13]. The grid needs to be clustered near to wall to capture the boundary layer on the airfoil at different angle of attacks.

The Reynolds number $Re = 3 \times 10^6$ with standard air properties at sea level have considered where the density $\rho = 1.225$ kg/m^3 at T = 288 k temperature and dynamic viscosity $\mu = 1.7894 \times 10^{-5}$ kg/ms. The airfoil chord was c = 1 cm, the inlet velocity V = 43 m/s The domain of the

Fig. 1 Morphed aerofoil nomenclature

Table 1 Morphing parameters

Parameter	Set 1			Set 2		
	Minimum	Maximum	Step	Minimum	Maximum	Step
δ_1	− 0.03	0	0.015	− 0.06	− 0.045	0.0075
E_1	0.2	0.4	0.1	0.2	0.4	0.1
δ_2	0	0.06	0.012	0	0.06	0.012
E_2	0.2	0.4	0.04	0.2	0.4	0.04

Fig. 2 a Stall angle of attack a_{stall} contour, $\delta_1 = 0$ to -0.03. **b** $\delta_1 = -0.045$ to -0.06
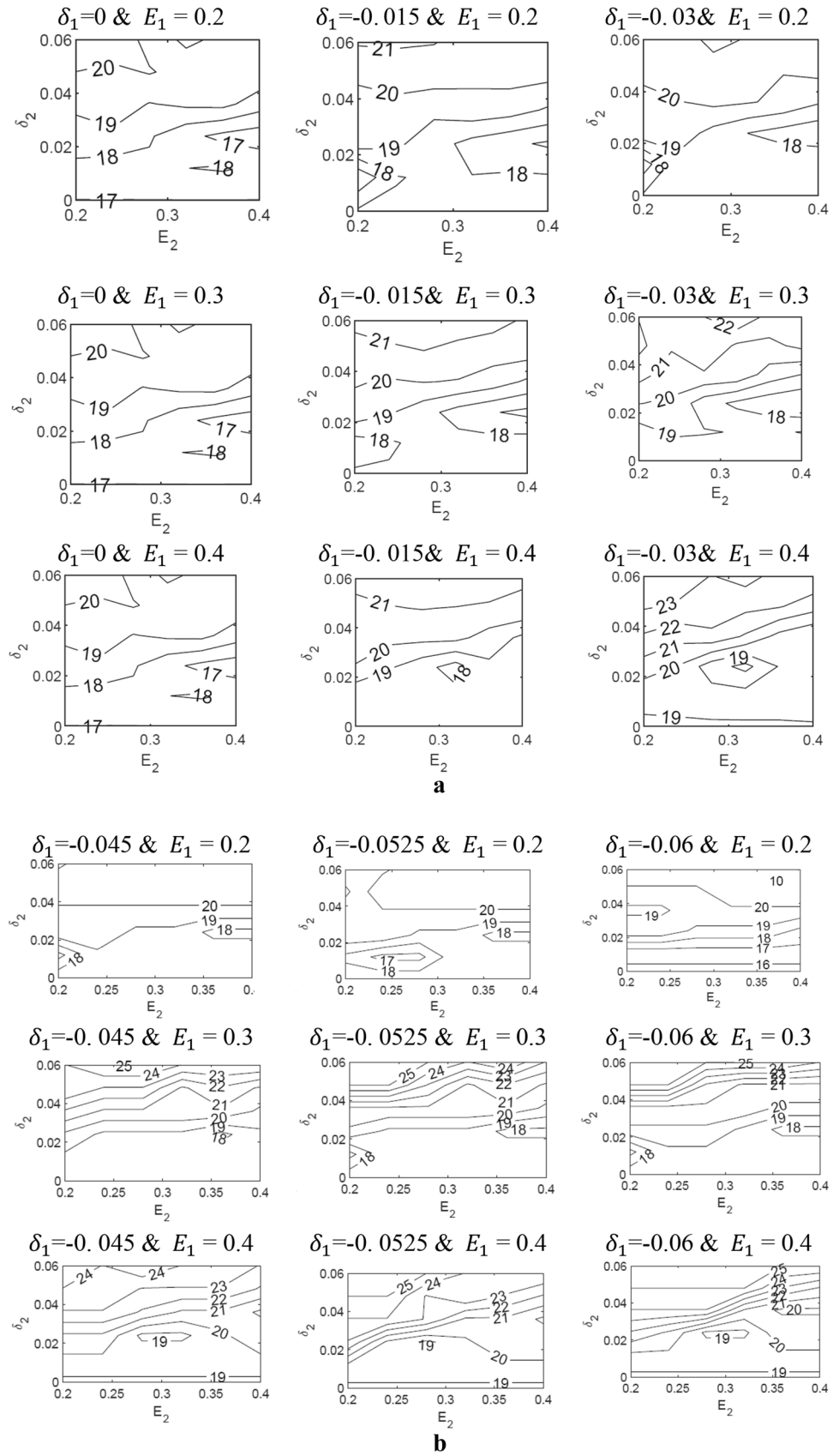
Fig. 3 **a** Maximum lift to drag ratio $C_L/C_{D_{max}}$ contour, $\delta_1 = 0$ to -0.03. **b** Maximum lift to drag ratio $C_L/C_{D_{max}}$ contour, $\delta_1 = -0.045$ to -0.06
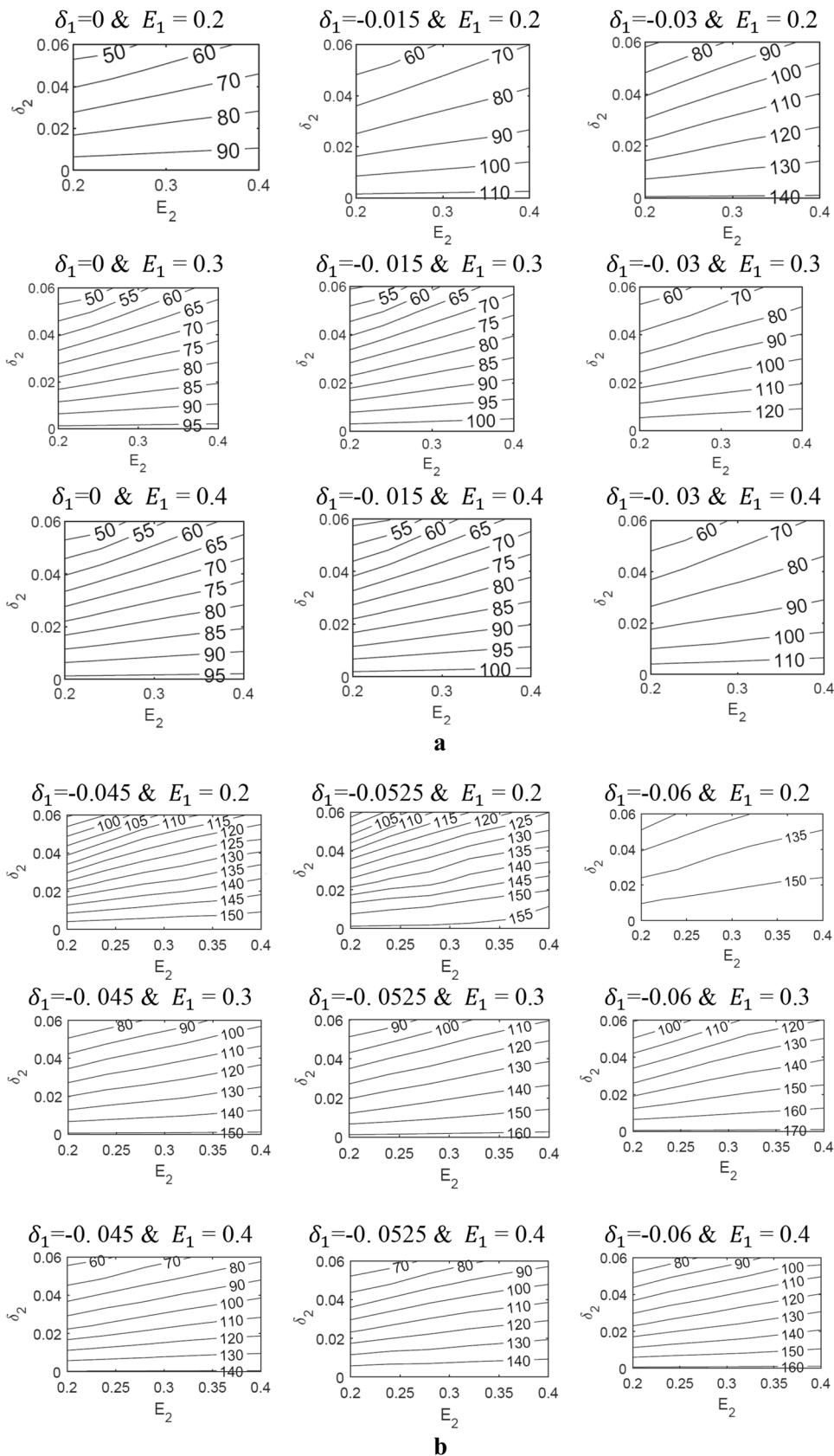
Table 2 Effect of trailing edge morphing length

Airfoil	δ_2	E_2	α_{stall}	$C_L/C_{D_{max}}$
Morphed1	0.06	0.2	20.62	45.29
Morphed2	0.06	0.4	19.74	62.23
Original	0	–	17	96

Table 3 Effect of leading edge morphing length

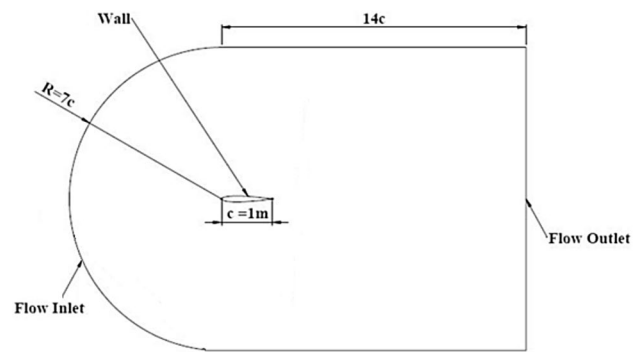| Airfoil	δ_1	E_1	α_{stall}	$C_L/C_{D_{max}}$
Morphed1	0.03	0.2	18.11	140
Morphed2	−0.03	0.4	18.86	116
Original	0	–	17	96

Fig. 4 Numerical model of NACA 0012 airfoil with domain boundary

Fig. 5 Unstructured grid used for the NACA 0012 airfoil

computational model is a half circle along its length with radius $7c$ extended with a square shape with $14c$ length. The two parallel side to the chord and the circle half is flow inlet velocity boundary (Drichlet value) and right side is pressure flow outlet (Gauge pressure) as shown in Fig. 4. The grid is unstructured consists of two regions, where the inner region is a circle with diameter equal to 3C. The mesh around the airfoil is cluster to capture the boundary layer Fig. 5. Turbulent model selected according to recommendations illustrated in Aziz et al. [14].

Ten computational grids of NACA 0012 airfoil with angle of attack equal to 10° to ensure grid convergence. The parameters details control the ten meshes presented in Table 5. The parameters (lift coefficient, Drag coefficient, Y+, etc.) varies with the number of grids are presented in Fig. 6 with 500 points on wall surface and a growth rate of 1.2. The grid at which number of cells independent on the results with optimized running time and fast stable convergence equal to 3.1×10^5 cells. Figure 7 presents the percentage in mass flow errors between inlet and outlet boundaries for the different angle of attack to insure the grid consistency.

5 Software validation with experiment

NACA 23012 was selected to validate experimentally the software used in simulation. The airfoil is simulated numerically for Spalart-Allmaras turbulence model Aziz et al. [14] and the result is compared with the experimental results

by the authors in Cairo University, aerospace laboratory. The load cell used in experiment has the rated load 10 kg, output: 1 mv/v, temperature zero drift: 0.1% F.S, the output sensitivity: ± 0.15 mv/v, temperature sensitivity: 0.05% F.S, insulation resistance: ≥ 2000 MΩ, and excitation voltage: 5–10 VDC Fig. 8a while the final assembly of force measuring mechanism presented in Fig. 8b. The complete setup inside the wind tunnel is presented in Fig. 9. The system was calibrated using weights to get the error in measurement. The average error in reading after calibration measurement was within 5%. In the experiment the results for airfoil NACA 23012 have measured from wind tunnel with the following setup: inlet velocity is equal to 16.389 m/s with standard air properties at sea level.

In the numerical simulation the Reynolds number $Re = 3 \times 10^6$ with standard air properties at sea level have considered. The airfoil chord was c = 20 cm, with the same inlet velocity considered in the experiment. The Spalar–Allmaras model has used involving wall-bounded

Table 4 Effect of leading and trailing edges morphing length

Case	δ_1	E_1	δ_2	E_2	α_{stall}	$C_L/C_{D_{max}}$
1	−0.06	0.2	0.06	0.2	20.83	92.73
2	−0.06	0.2	0.06	0.4	20.83	130.4
3	−0.06	0.4	0.06	0.2	25	70.31
4	−0.06	0.4	0.06	0.4	25	93.95

Table 5 The mesh shape controlled parameters

Computational grids number	1	2	3	4	5	6	7	8	9	10
Max face size $\times 10^{-3}$	40	20	10	9.5	9	8.5	8.5	8	7.5	5
Near wall patch thickness $\times 10^{-2}$ (m)	1.2	5	7.5	7.5	1	1	1	1	1	1
Total number of cells $\times 10^5$	1.2	1.4	2.6	2.7	2.9	3.1	3.3	3.4	3.7	7.1
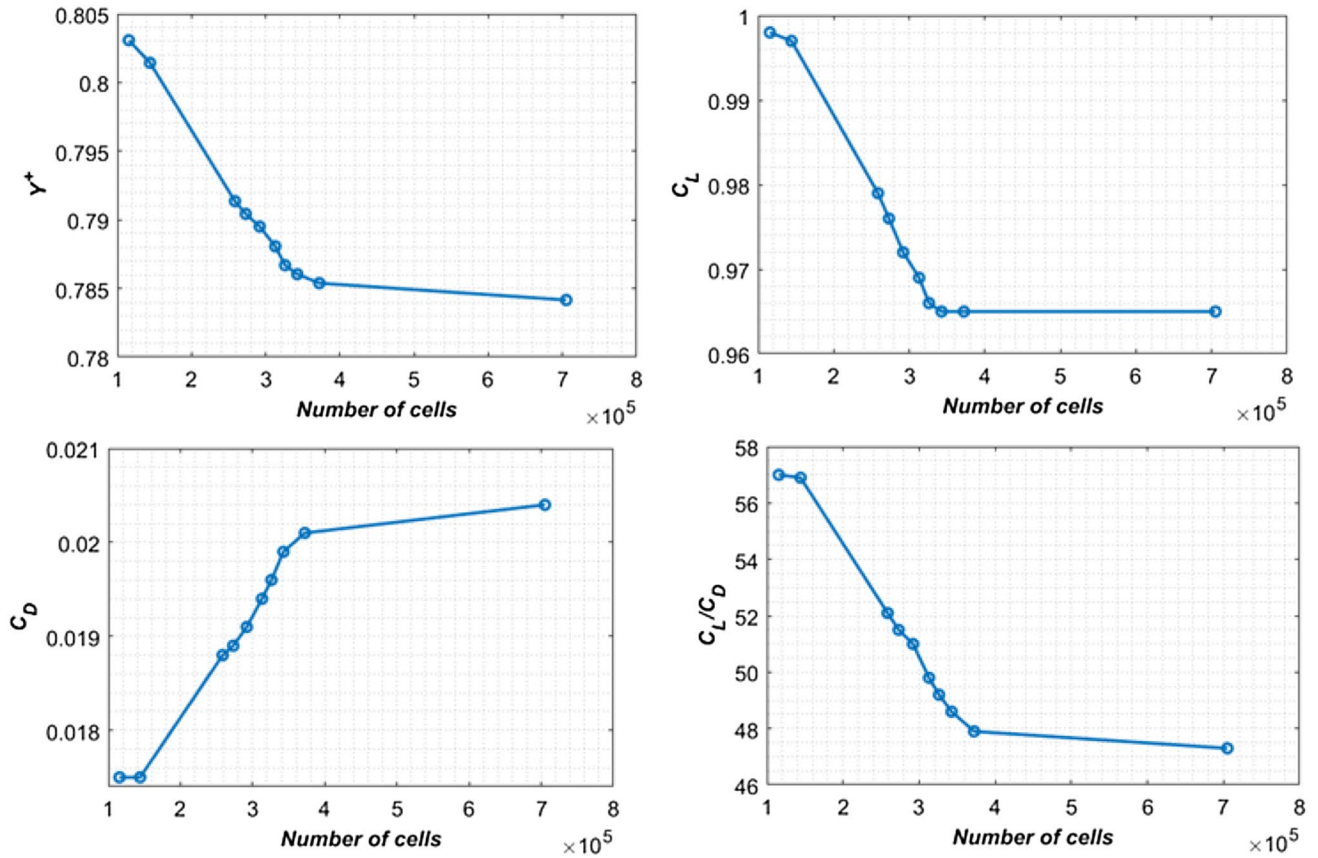
Fig. 6 Variation of the aerodynamics coefficients and Y+ with the number of cells at angle of attack equal to 10°
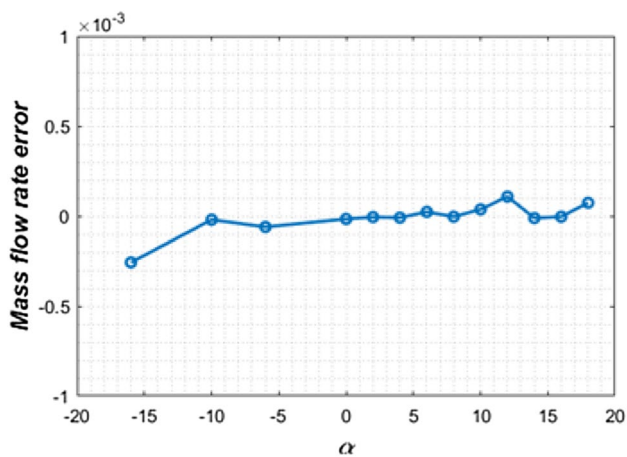
Fig. 7 Percentages in mass flow errors between inlet and outlet boundaries for the different angle of attack
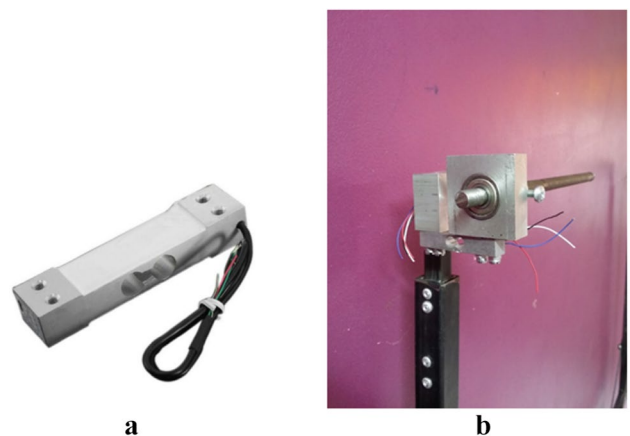
Fig. 8 Load cell (**a**) final assembly of force measuring mechanism (**b**)

Fig. 9 Wind tunnel's test section

flows. This model has shown good results for boundary layers subjected to adverse pressure gradients. The comparisons between the numerical simulations and the experiment results at different angles of attack are presented in Fig. 10.

The Wind tunnel (WT) validation on NACA 23012 is performed because of the availability of the experimental data. To match these data with the results of the numerical simulations the numerical setup including mesh sizing and turbulence model were the same for NACA 0012 which is easier handled during geometry variations with introducing the new morphing parameters.

6 Parametric study

The parametric studies using numerical simulations with ANSYS Fluent have conducted based on the results previously obtained by the X-FOIL imported to MATLAB.

The morphed airfoil shapes used in the numerical simulations have selected corresponding to the maximum important aerodynamics coefficients of the airfoil such $C_{L_{MAX}}$, $(C_L/C_D)_{MAX}$ and maximum stall angle. The morphed shapes characteristics are compared with the basic shape of NACA 0012. The parametric study performed for each variable alone that gives a modified shape of the basic airfoil corresponding to the maximum value for this parameter.

7 Maximum stall angle α

The morphed airfoil shape that matches the maximum stall angle of attack obtained by X-FOIL imported in MATLAB calculations is presented in Fig. 11.

The stall angle of attack for basic airfoil was 16° that gave a maximum coefficient of lift equal $C_{L_{MAX}} = 1.23$ while the morphed airfoil stall angle was 20° the stall angle increased by 25% but the maximum coefficient of lift equal $C_{L_{MAX}} = 0.833$ decreased by 32.28% Fig. 12.

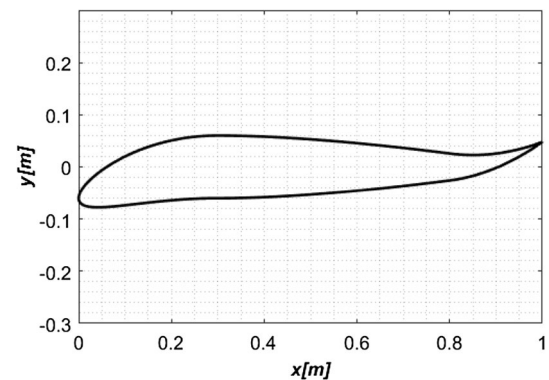Figure 13 illustrates Coefficient of drag C_D versus angle of attack α for basic and morphed airfoils. The morphed

Fig. 11 Morphed airfoil matched maximum stall angle α

Fig. 10 Calculated and experimental aerodynamic lift coefficient results
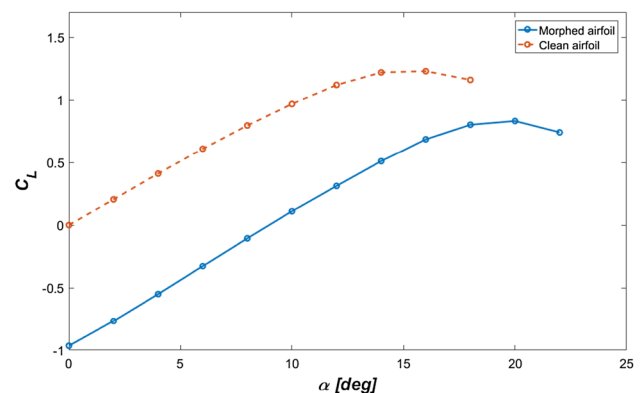

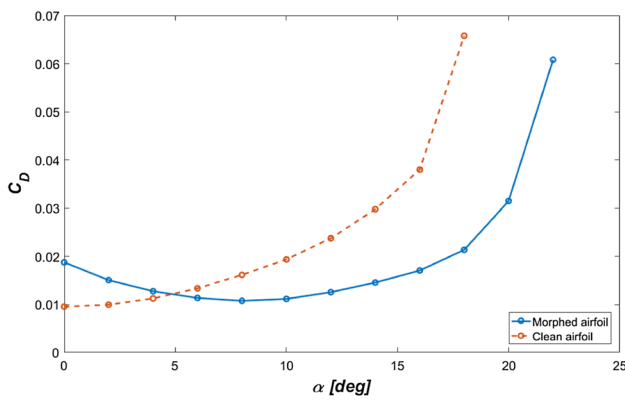**Fig. 12** Lift coefficient for basic and morphed airfoils

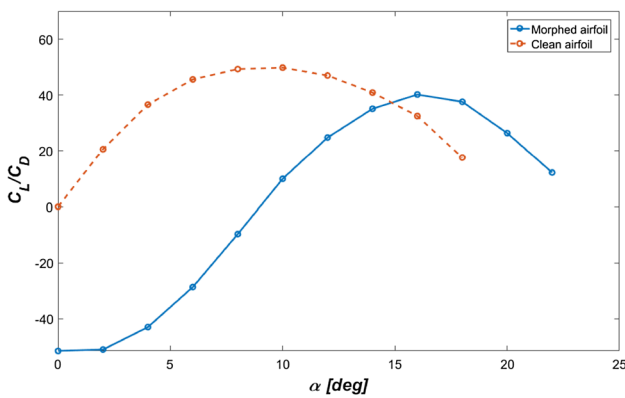**Fig. 13** Drag coefficient for basic and morphed airfoils

Fig. 14 Lift to drag ratio for basic and morphed airfoils

contribution at high angle of attacks gives lower coefficient of drag values. Figure 14 shows C_L/C_D ratio for basic and morphed airfoil the maximum C_L/C_D for basic airfoil is 49.8 at 10° angle of attacks while the morphed airfoil gave 40.2 at 16° angle of attack.

Figures 15 and 16 show the velocity and pressure contours respectively for both basic NACA 0012 airfoil and morphed airfoils corresponding to maximum stall angle. The simulation conducted at angle of attack equals 16°. For the basic airfoil the separation point starts at 65.56% of the chord total length while the morphed airfoil has no notable separation because it is still far from the stall limit.

8 Maximum lift to drag ratio C_L/C_D

The morphed airfoil shape that matches $\left(C_L/C_D\right)_{MAX}$ corresponding to 11.6° angle of attack obtained by X-FOIL imported in MATLAB calculations are shown in Fig. 17.

The numerical simulation for the considered airfoil indicates increase in lift coefficient up to 8.13% compared to basic airfoil lift coefficient Fig. 18. The lift coefficient for the basic airfoil equal 1.23 corresponding to stall angle equals 16°. The lift coefficient for the morphed airfoil equals 1.33 corresponding to stall angle equals 18°. The contribution of morphed airfoil gave lower coefficient of drag than the basic airfoil Fig. 19. The morphed airfoil gave the maximum value for $C_L/C_D = 52.9$ at angle of attack equals 10° increased by 6.22% compared to basic airfoil Fig. 20.

Figures 21 and 22 shows the velocity and pressure contours respectively for both basic NACA 0012 airfoil and Morphed airfoil that shows morphing produced better performance than the basic airfoil from the separation point
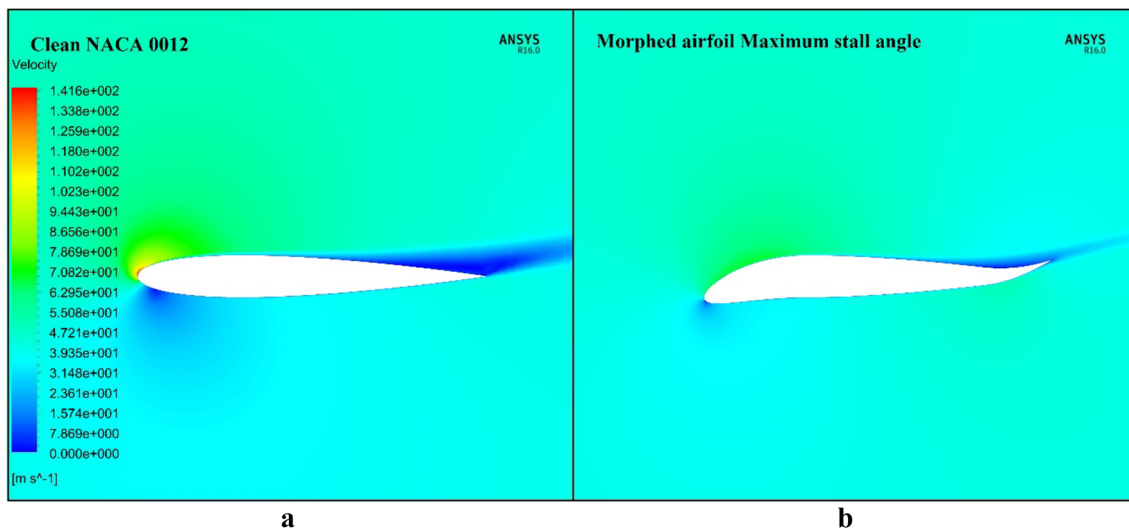

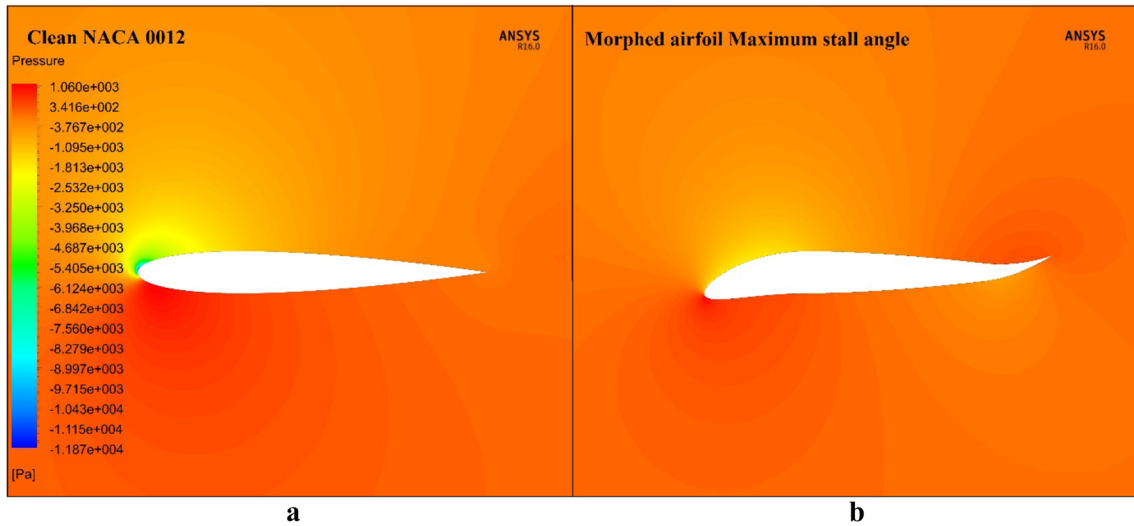**Fig. 15** Velocity contours for basic (**a**) and morphed (**b**) airfoils at 16° angle of attack

Fig. 16 Pressure contours for basic (**a**) and morphed (**b**) airfoils at 16° angle of attack
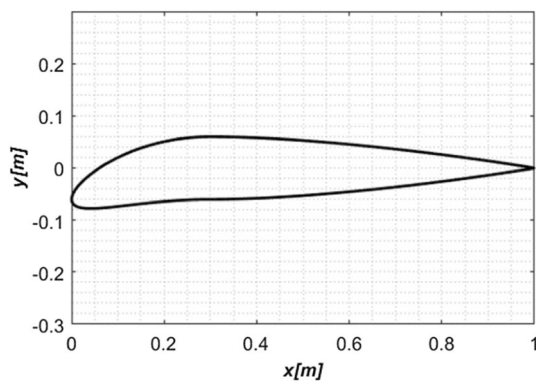

Fig. 17 Morphed airfoil matched $(C_L/C_D)_{MAX}$
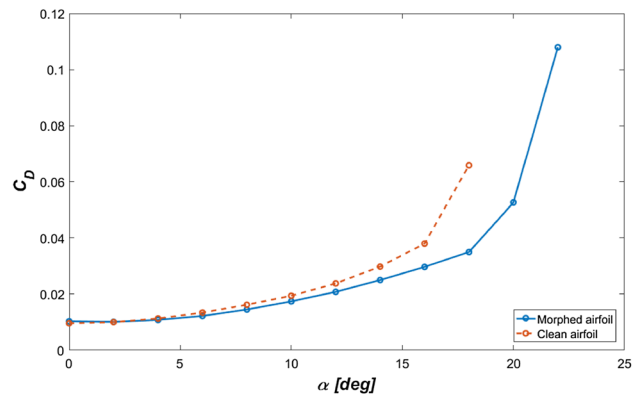

Fig. 19 Drag coefficient for basic and morphed airfoils
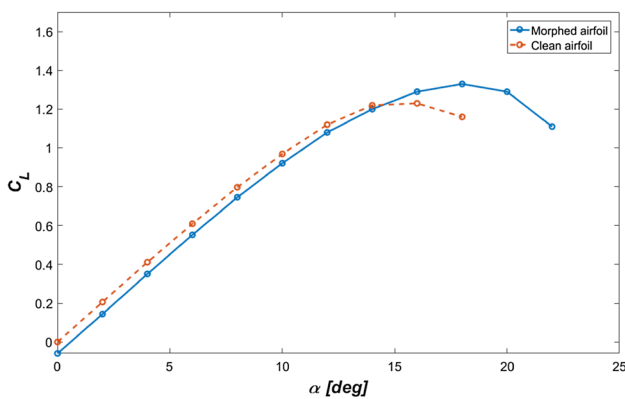

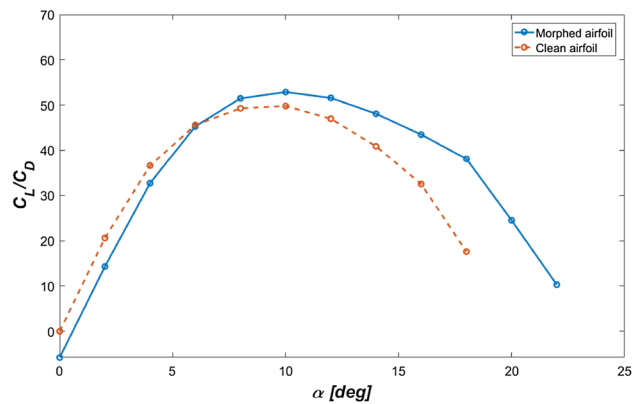**Fig. 18** Lift coefficient for basic and morphed airfoils

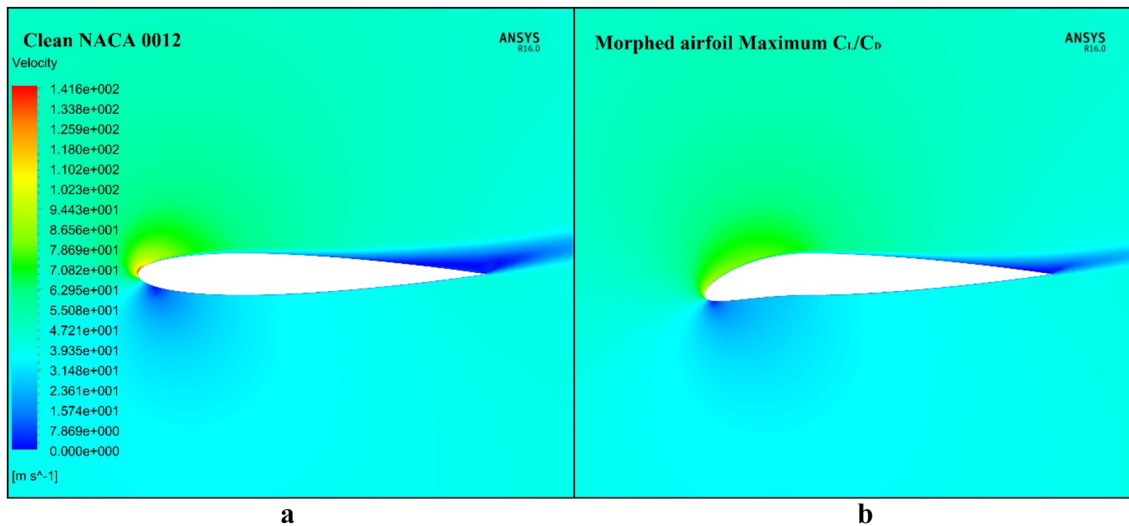**Fig. 20** Lift to drag ratio for basic and morphed airfoils

Fig. 21 Velocity contours for basic (**a**) and morphed (**b**) airfoils at 16° angle of attack
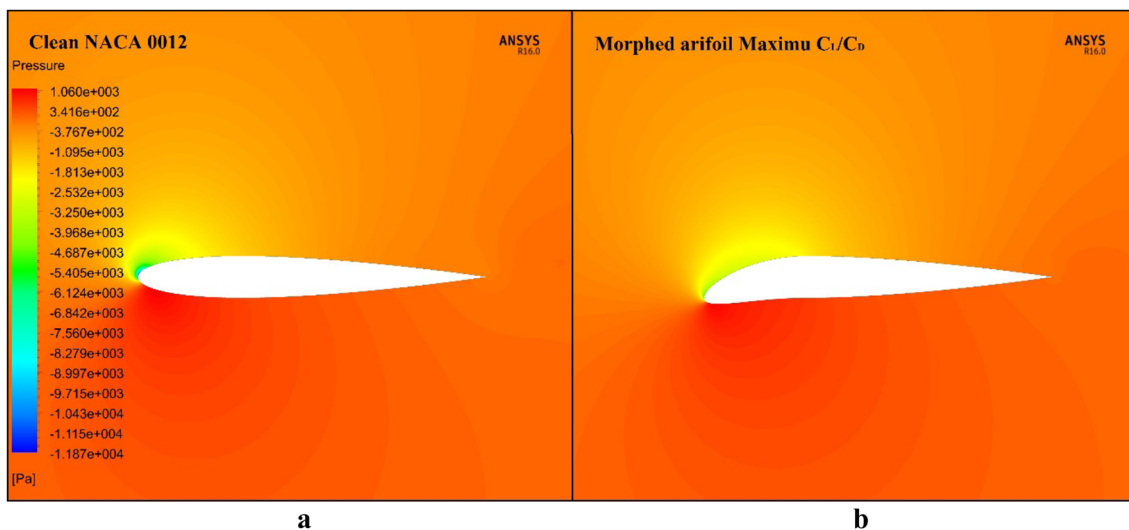

Fig. 22 Pressure contour for basic (**a**) and morphed (**b**) airfoils at 16° angle of attack
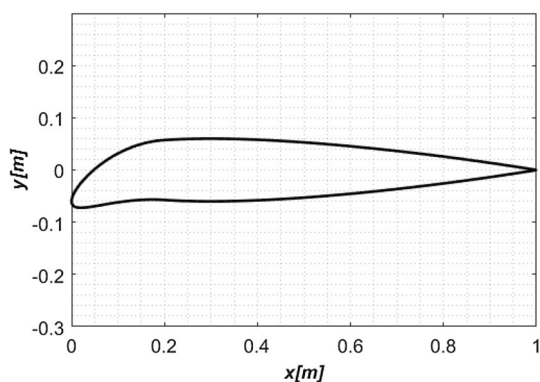

Fig. 23 Morphed airfoil matched maximum C_L

of view. For the basic airfoil the separation point starts at 65.56% of the chord total length while the morphed airfoil separation point starts at 83.51% from the chord total length. This explains the more lift coefficient compared to basic airfoil at the same angle of attack.

9 Maximum lift coefficient $C_{L_{MAX}}$

The morphed airfoil shape that matches the maximum $C_{L_{MAX}}$ obtained by X-FOIL imported in MATLAB a calculation is shown at Fig. 23.

The airfoil shape shown in Fig. 23 improved the coefficient of lift C_L to its maximum value equal $C_L = 1.34$ at 18° stall angle of attack while the basic airfoil gave coefficient
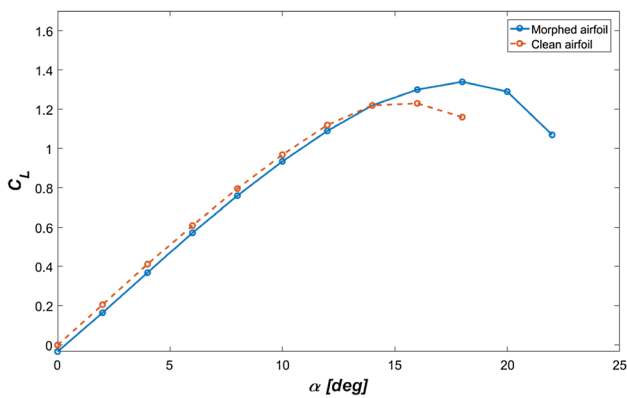
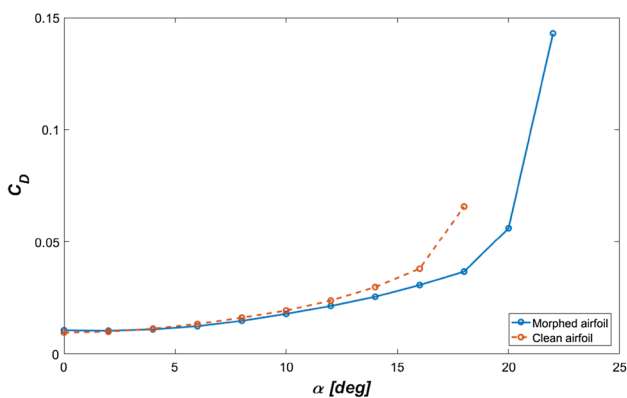**Fig. 24** C_L versus α for basic and morphed airfoils

Fig. 25 C_D versus α for basic and morphed airfoils
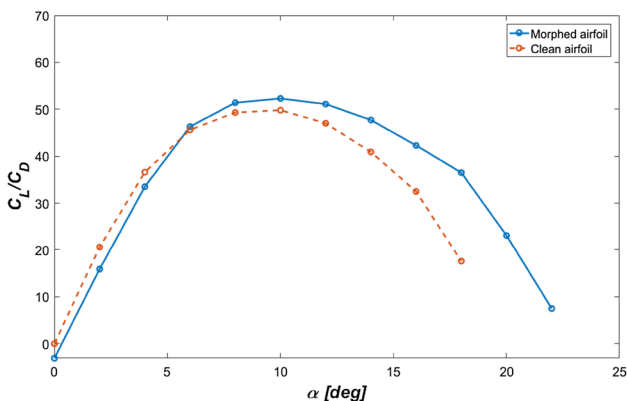

Fig. 26 C_L/C_D versus α for basic and morphed airfoils

of lift equal C_L = 1.23 at lower stall angle of attack equal 16° increased by 11% from the basic airfoil the data of both airfoils shown at Fig. 24.

The contribution of coefficient of drag C_D nearly the same as C_L/C_D contribution giving lower values than the basic airfoil the data is shown at Fig. 25. The maximum C_L/C_D for the

morphed airfoil gave 5.02% increase more than the basic airfoil all data illustrated at Fig. 26.

Figures 27 and 28 show the velocity and pressure contours respectively for both basic NACA 0012 airfoil and Morphed (Maximum C_L). for the basic airfoil the separation point starts at 65.56% chord length while the morphed airfoil separation starts at 93.85% chord length.

10 Controlled C_L using morphed airfoils

The morphed airfoil shapes corresponding to maximum C_L at different angle of attack are shown in Fig. 29.

In order to maximize the performance of the wing at all flight regimes (different angle of attacks) the airfoil shape of the wing will be changed according to its angle of attack to give the maximum certain aerodynamic characteristics such as (C_L) that is called controlled C_L.

Figure 30 illustrates lift coefficient C_L comparison between basic and controlled C_L airfoils at every angle of attack. The result has indicated that controlled C_L morphed airfoil gave a better aerodynamic characteristics compared to basic airfoil at high angle of attacks.

11 Conclusions

The current study has introduces the variations in aerodynamic characteristics due to airfoil morphing including droop nose and trailing edge morphing. The morphed airfoil configuration parameterization facilitates the parametric study. The combined effect of droop nose and trailing edge morphing was studied. The results from the X-FOIL showed increase in stall angle up to 26° and lift to drag ratio up to 120. The numerical simulation study with ANSYS performed which targeted different important aerodynamic parameter improvement. From the maximum stall angle point of view the results showed increase of stall angle up to 20° and lift to drag ratio increased up to 6.22% compared to basic airfoil at separate morphed shapes. Also the separation has delayed to 75.12% of the chord length. While for the basic airfoil the separation starts at 66.4%. From the maximum Lift to drag ratio C_L/C_D point of view the morphed airfoil gave the maximum value for C_L/C_D= 52.9 at angle of attack equal 10° increased by 6.22% from the basic airfoil. Also the separation has delayed to 84.14% of the chord length. From the maximum lift coefficient point of view the lift coefficient increased also up to 1.34. Also the separation has delayed to 83.39% of the chord length. This study has showed a level of success while controlling the airfoil morphing associated with certain
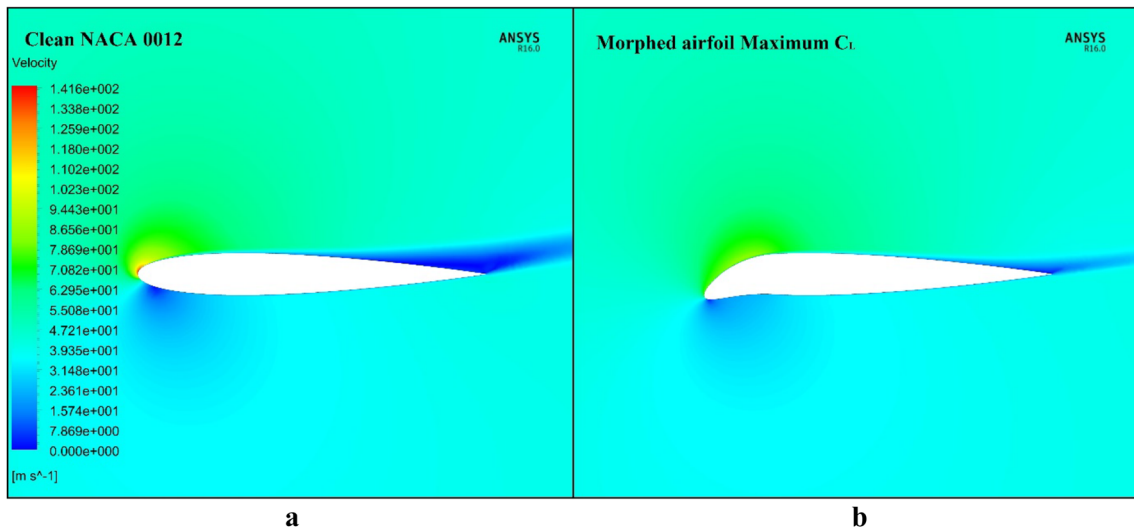
Fig. 27 Velocity contours for basic (**a**) and morphed (**b**) airfoils at 16° angle of attack
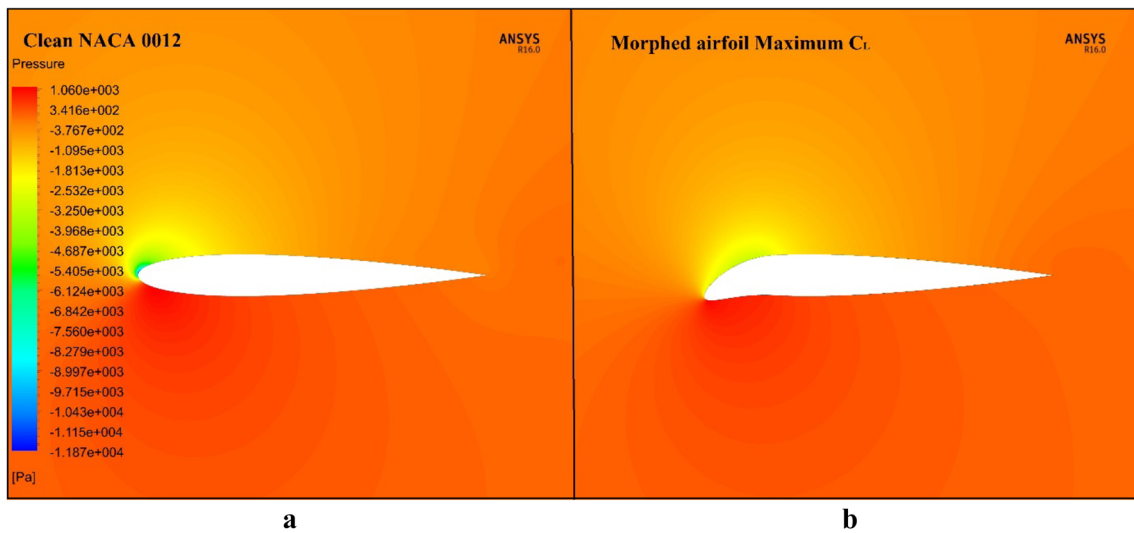

Fig. 28 Pressure contours for basic (**a**) and morphed (**b**) airfoils at 16° angle of attack
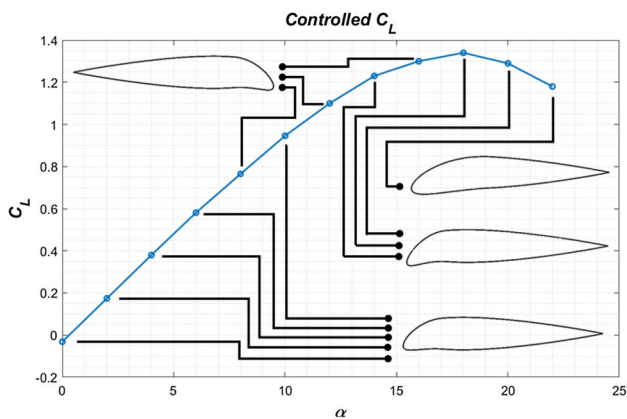

Fig. 29 C_L versus α graph for controlled C_L and airfoil shapes for every angle of attack
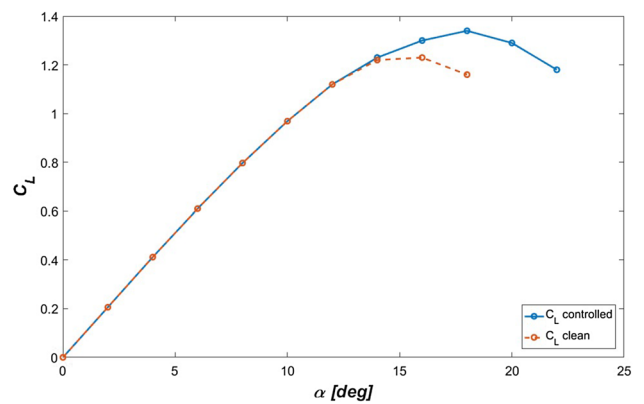
Fig. 30 C_L values for basic and maximum C_L airfoils

aerodynamic condition such maximum lift coefficient during the variety of operating angle of attack.

Compliance with ethical standards

Conflict of interests The authors declare that they have no conflict interest.

References

1. Yue T, Zhang X, Wang L, Ai J (2017) Flight dynamic modeling and control for a telescopic wing morphing aircraft via asymmetric wing morphing. Aerosp Sci Technol 70:328–338
2. Kamliya Jawahar H, Ai Q, Azarpeyvand M (2017) Experimental and numerical investigation of aerodynamic performance of airfoils fitted with morphing trailing-edges. In: 23rd AIAA/CEAS aeroacoustics conference, p 3371
3. Gamble LL, Pankonien AM, Inman DJ (2017) Stall recovery of a morphing wing via extended nonlinear lifting-line theory. AIAA J 55:2956–2963
4. Kimaru J, Bouferrouk A (2017) Design, manufacture and test of a camber morphing wing using MFC actuated mart rib. In: 2017 8th international conference on mechanical and aerospace engineering (ICMAE). IEEE, pp. 791–796
5. Vale J, Afonso F, Oliveira É, Lau F, Suleman A (2017) An optimization study on load alleviation techniques in gliders using morphing camber. Struct Multidiscip Optim 56(2):435–453
6. Jodin G, Motta V, Scheller J, Duhayon E, Döll C, Rouchon JF, Braza M (2017) Dynamics of a hybrid morphing wing with active open loop vibrating trailing edge by time-resolved PIV and force measures. J Fluids Struct 74:263–290
7. Vasista S, Riemenschneider J, van de Kamp B, Monner HP, Cheung RC, Wales C, Cooper JE (2016) Evaluation of a compliant droop-nose morphing wing tip via experimental tests. J Aircr 54(2):519–534
8. Afonso F, Vale J, Lau F, Suleman A (2017) Performance based multidisciplinary design optimization of morphing aircraft. Aerosp Sci Technol 67:1–12
9. Wu M, Xiao T, Ang H, Li H (2017) Investigation of a morphing wing solar-powered unmanned aircraft with enlarged flight latitude. J Aircr 54(5):1996–2004
10. Zhang W, Chen LL, Guo XY, Sun L (2017) Nonlinear dynamical behaviors of deploying wings in subsonic air flow. J Fluids Struct 74:340–355
11. Hu W, Yang Z, Gu Y, Wang X (2017) The nonlinear aeroelastic characteristics of a folding wing with cubic stiffness. J Sound Vib 400:22–39
12. Günel O, Koç E, Yavuz T (2016) CFD vs. XFOIL of airfoil analysis at low reynolds numbers. In: 2016 IEEE international conference on renewable energy research and applications (ICRERA). IEEE, pp 628–632
13. Ariff M, Salim SM, Cheah SC (2009) Wall y+ approach for dealing with turbulent flow over a surface mounted cube: part 1—low Reynolds number. In: Seventh international conference on CFD in the minerals and process industries, pp 1–6
14. Aziz MA, Elsayed AM (2015) CFD Investigations for UAV and MAV low speed airfoils characteristics. Int Rev Aerosp Eng 8(3):95–100

Publisher's Note Springer Nature remains neutral with regard to jurisdictional claims in published maps and institutional affiliations.